ELSEVIER

Thermochimica Acta 391 (2002) 97–106

thermochimica acta

www.elsevier.com/locate/tca

The role of the temperature errors in DSC scans on the prediction of the average density of nuclei in polymers crystallized under quiescent conditions

J.A. Martins[a,*], M.J.A. Malheiro[a], J.C. Teixeira[b], J.J.C. Cruz Pinto[c]

[a]*Departamento de Engenharia de Polímeros, Universidade do Minho, Campus de Azurém, 4800-058 Guimarães, Portugal*
[b]*Departamento de Engenharia Mecânica, Universidade do Minho, Campus de Azurém, 4800-058 Guimarães, Portugal*
[c]*Departamento de Química, Universidade de Aveiro, 3810-193, Aveiro, Portugal*

Received 10 September 2001; received in revised form 26 November 2001; accepted 12 December 2001

Abstract

Following the results of previous works, the methodology used to perform DSC temperature calibrations on cooling from the melting onsets of pure metal standards is briefly presented, together with a discussion of the errors involved. The average true sample temperature in non-isothermal scans is evaluated, and the sample's thermal resistance and release of the heat of crystallization duly accounted for. The importance of the above temperature corrections in the definition of a temperature corresponding to half of the phase change in non-isothermal scans is also analyzed when predicting the average density of nuclei in polymer quiescent crystallization experiments at constant cooling rate. Additional sources of error, such as the effect of the sample's thickness and the temperature profile within the sample are also briefly discussed.

Keywords: Calibration; Cooling; Thermal lag; Sample's thickness

1. Introduction

Thermal analysis data, in general, and differential scanning calorimetry data, in particular, require several temperature corrections, in order to obtain meaningful thermophysical properties of the samples under analysis. Several workers have given important contributions, among which stand, in the field of the differential scanning calorimetry, those of Richardson [1,2] and Höhne et al. [3].

The errors with which the calibration on cooling is performed, the accurate evaluation of the sample's thermal resistance, and the effect that the temperature profile across the sample may have in the recorded scans (such as in those resulting from non-isothermal crystallization or enthalpic relaxation) are of importance in the evaluation of the average true sample temperature. Together with a very careful sample preparation, a separate evaluation of all possible error sources is then required.

The importance of these temperature corrections and the evaluation of the average true sample temperature will be illustrated in this work, by the use that is possible to make of non-isothermal DSC scan results to predict the average density of nuclei in

* Corresponding author. Tel.: +351-253-510245; fax: +351-253-510249.
E-mail address: jamartins@dep.uminho.pt (J.A. Martins).

0040-6031/02/$ – see front matter
PII: S0040-6031(02)00167-3

polymer quiescent crystallization experiments. The procedure presented here was extended in another work to predict the average density of nuclei and spherulite size in real processing conditions, particularly for rotational mouldings [4].

It was previously shown that the calibration on cooling could be performed from calibration data on heating, using standard metals [5]. The errors in performing this calibration were discussed in the above reference and compared with work published by other authors [6], where liquid crystalline transitions of high-purity liquid crystals were used to calibrate on cooling. The two basic steps involved in the procedure are the separate evaluation of an isothermal correction and of a rate-dependent thermal lag. The isothermal correction is the same for all scanning modes and rates, while the rate-dependent thermal lag is symmetrical for heating and cooling experiments. This symmetry may easily be checked in liquid crystalline transitions, where it is also possible to recognize that, even with high-purity liquid crystals, a strictly non-zero supercooling is always detected. This supercooling is small, often less than 0.3 °C, as it may be shown by an accurate evaluation of the parameters involved in the calibration on cooling.

As shown previously [5], the true temperature during a cooling scan, corrected for the isothermal correction and the rate-dependent thermal lag, may be evaluated from the melting onsets of two pure metal standards by

$$T_t^- = (2 - a^+)T_m - b^-, \tag{1}$$

with $b^- = 2\,\Delta T_o + b^+$. T_m is the measured temperature; a^+ and b^+ are, respectively, the slope and the intercept of the calibration line at a particular heating rate (the same as the one used for cooling); and ΔT_o is the isothermal correction. A more exact expression has also been developed [7,8], that nevertheless, yields almost identical results.

The above temperature is the true sample temperature of a pure substance, with high thermal conductivity. However, in samples with lower thermal conductivity, such as polymer samples, an additional thermal lag due to the sample's thermal resistance must be evaluated, which is dependent on the sample's thermal history, on its thickness and area, and on the sample's encapsulation mode (hand- or press-crimped pans). For example, if a sample disk is extracted from an extruded polymer plate and the sample is encapsulated in a press-crimped pan, the decrease of sample's contact area and increase of thickness, as a result of chain rearrangements to more entropic states after melting, may lead to unrealistic values for the sample's thermal resistance. A common procedure to make this evaluation is by performing scans with indium, and then indium over a polymer sample. For each peak, the slope of its ascending part is evaluated, and the sample's thermal resistance (R_s) is obtained from the difference between the reciprocal of the two slopes.

For the evaluation of the average true sample temperature during the non-isothermal crystallization of polymers, an additional correction is required, due to the release of the heat of crystallization during solidification [9]. Taking in account these two corrections, the average true temperature of the crystallizing sample is given by

$$(T_t^-)_s = T_t^- + \left(|\Delta h_c| m_s R_s \frac{dX}{dt} - m_s \bar{c}_p R_s \frac{d(T_t^-)_s}{dt} \right), \tag{2}$$

where m_s is the sample's mass; dX/dt the rate of solid phase formation; $|\Delta h_c|$ the total enthalpy released per unit mass; $\bar{c}_p$ the sample's specific heat capacity; and R_s the apparent thermal resistance at a particular cooling rate (dT/dt); and T_t^- is the true sensor temperature, given by Eq. (1). Eq. (2) may be more accurately solved as a first-order ordinary differential equation, which it really is, or assuming that the rate of variation of $(T_t^-)_s$ with time is approximately given by the programmed scanning rate. For the purpose of the evaluation of the average true sample temperature, only the thermal resistance corresponding to half of the sample's thickness will be used here, i.e. $R_s/2$.

Knowing the average true sample temperature during a non-isothermal cooling, run at a particular scanning rate, it is possible to evaluate, for each cooling rate, the sample temperature corresponding to half of the phase change, $T_{50\%}$. This temperature may then be used to estimate the average density of nuclei in non-isothermal quiescent crystallization experiments [4,10].

The basis of this estimate is the experimental evidence that the slope of the logarithm of the growth rate of the spherulites, as measured in a hot-stage

optical microscope, versus $1/T\,\Delta T$ (where ΔT is the supercooling) is lower than the slope of the logarithm of the reciprocal of the crystallization half-time, as measured from isothermal DSC experiments. An explanation for this was provided, being in fact related to the temperature dependence of the average density of nuclei (number of nuclei activated at a particular crystallization temperature per unit volume). This dependence is accounted for in the relationship between the reciprocal of the half of crystallization time and the growth rate, which, for Avrami's equation and an instantaneous nucleation of spheres, is

$$\frac{1}{t_{50\%}} = \left(\frac{k}{\ln 2}\right)^{1/3} = (C\bar{N})^{1/3} G, \tag{3}$$

where $C = 4\pi\rho_s/(3\rho_l \ln 2)$; $\bar{N}$ is the average number of nuclei per unit volume of untransformed material; ρ_s and ρ_l are the densities of the solid and liquid phases, respectively; and G is the spherulite linear growth rate. The temperature dependence of G is assumed to be the one predicted from Lauritzen and Hoffman's theory of the secondary nucleation [11]. The temperature dependence of the average density of nuclei was established in a previous work [12] by assuming an ideal solution between embryos and polymer chain segments in a favorable conformational state to be added to a semicrystalline embryo (N_s), which is

$$\bar{N}_t = N_s \exp\left(-\frac{K_n}{T\,\Delta T}\right), \tag{4}$$

where $K_n = 4b_o\sigma\sigma_e T_m^0/(k_B\,\Delta H_f^\circ)$, and $\bar{N}_t = (\rho_s/\rho_l)\bar{N}$ is the average number of nuclei per unit volume of transformed material. A consequence of this temperature dependence is that data on the crystallization half-times cannot be used to evaluate the folding and lateral surface energies, σ_e and σ, respectively.

Assuming an instantaneous nucleation, the inclusion of the temperature dependence of the average density of nuclei and the temperature dependence of G into the reciprocal of the crystallization half-time yields

$$\bar{N}_t = \frac{1}{C_t}\exp\left\{-3(K_g^{1/t_{50\%}} - K_g^G)\frac{1}{T\,\Delta T f} + 3\left[\ln\left(\frac{1}{t_{50\%}}\right)_o - \ln(G)_o\right]\right\}, \tag{5}$$

with $C_t = (\rho_l C/\rho_s)$, as a result of the conversion to average density of nuclei per unit volume of transformed material. The intercepts, $\ln(1/t_{50\%})_o$ and $\ln(G)_o$, are evaluated by a linear fit over the DSC and optical microscopy experimental data. $K_g^{1/t_{50\%}}$ and K_g^G are, respectively, the slopes of $\ln(1/t_{50\%})$ and $\ln(G)$ versus $1/T\,\Delta T f$.

2. Experimental

The thermal analysis experiments were performed using a Perkin-Elmer DSC-7, with a purge-gas rate of 20 cm^3/min. The temperature of the cold block was kept constant at 5 °C. The standard metals used to perform the calibration were indium (purity 99.99999%), tin (purity 99.9999%), and lead (purity 99.99%) from Goodfellow; and zinc, supplied by Perkin-Elmer, with an unspecified purity. A liquid crystal HP-53 (4-(4-pentyl-cyclohexyl)-benzoic acid-4-propyl-phenil ester), supplied by Merck, with the transitions indicated in Fig. 1, was used to check the calibration on cooling and to quantify the errors with which it was performed. Samples of around 4 mg of the standard metals and liquid crystal were encapsulated in 30 μl aluminum pans with holes, which were used for all experiments performed in this work. Due to the several liquid crystalline transitions occurring in the temperature interval

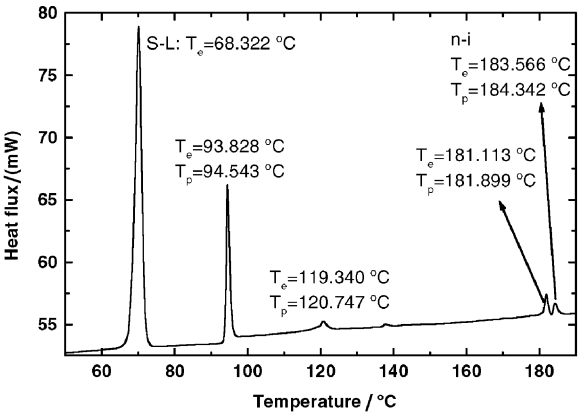

Fig. 1. Observed transitions of the liquid crystal HP-53. The solid–liquid (S–L) and the nematic–isotropic (n–i) transitions are indicated. The scan was performed, after calibration at 16 °C/min (with baseline at the same scanning rate), with a sample of 4.515 mg in a 30 μl aluminum pan with holes. An additional transition at 136.82 °C is not indicated in the figure.

between 90 and 185 °C, this material seems to be a good candidate to perform, or to check, temperature calibrations in the cooling mode, as suggested by Sarge et al. [13].

The average density of nuclei was predicted as a function of the cooling rate for a rotational moulding grade of polypropylene, Borealis BE 182 B, with a melt flow index of 13 g/10 min and $T_m^0 = 176.75$ °C. The samples used had a thickness of 0.4 mm and a mass of approximately 8 mg. Since the melting temperature of this material is similar to that of the indium standard, the evaluation of the thermal lag between the sample bottom and top surfaces, and of its scanning rate dependence was not possible.

For this purpose, samples of MDPE (from Enichem, RP264H, with $\bar{M}_w = 31000$ g/mol, $T_m^0 = 143$ °C), with varying thickness and constant area, were encapsulated in aluminum pans and used. The samples' area and thickness were measured before and after the experiments. The thermal lag between the bottom and top of the polymer samples was measured by the difference in the melting onsets of indium and indium over a polymer sample. Identical pans and indium samples were used in all of these experiments.

3. Critical presentation of the results

The results of Fig. 2a and b show the melting and crystallization onset temperatures of tin before and after calibration, respectively. The upmost curve in Fig. 2a shows the expected increase of the melting onset temperature with the scanning rate. This thermal lag is due to the small sample's thermal resistance and the thermal resistances of the oven and the aluminum pan. It increases with the scanning rate, and its extrapolation to zero scanning rate allows the evaluation of the isothermal correction, which, due to non-linearities in the temperature sensor reading, may vary with temperature. For the melting temperature of tin, the isothermal correction was only −0.82 °C, while for the melting temperature of indium, it was −1.10 °C. This isothermal correction also changes with the operating conditions of the instrument, being possible to set it to zero by hardware adjustment. The error bars in Fig. 2a represent the maximum deviation around a mean value after three consecutive scans at the same scanning rate and with the same sample.

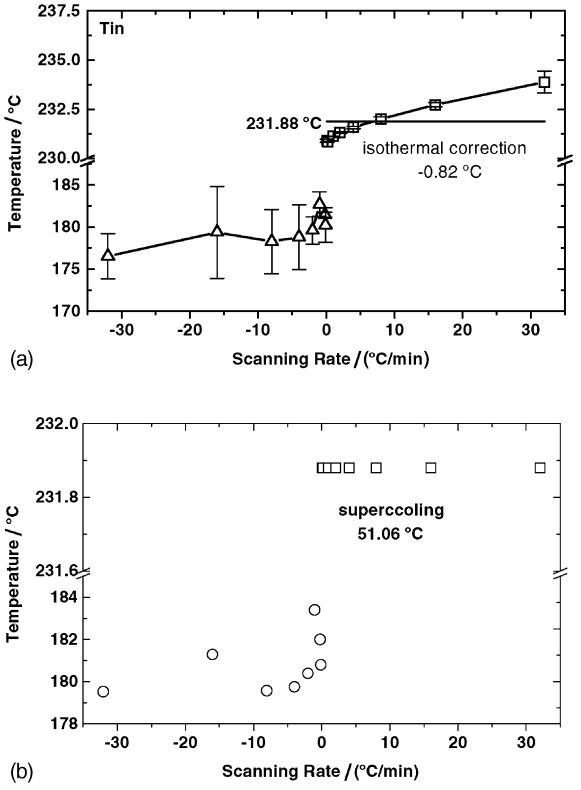

Fig. 2. Melting and crystallization onset temperatures of Sn at the indicated scanning rates: (a) before calibration; (b) after calibration, both on heating and cooling.

After the calibration on heating and cooling, using the melting onsets of indium and tin at the same scanning rates, the mean values of Fig. 2a are corrected for the isothermal correction (the same for heating and cooling experiments) and for the rate-dependent thermal lag, the results being shown in Fig. 2b.

Tin crystallizes with a high supercooling, ca. 51 °C for a cooling rate as low as −0.1 °C (the minimum experimentally accessible), and one could possibly argue that this supercooling would be very much smaller if melting runs could be carried out, and yield measurable results on a DSC, at lower cooling rates. After the calibration on cooling, as expected, the crystallization onsets decreased somewhat regularly with the cooling rate to an apparent minimum plateau of ca. 179.5 °C. However, an evaluation of the accuracy with which the calibration on cooling is performed with this material would require explicitly

accounting for the crystallization supercooling (through an adequate formulation of the nucleation phenomena), in addition to the heat released during its crystallization (through the application of Eq. (2)). Neglecting this second (possibly much less significant) effect, one may look at the data on the lower part of Fig. 2b as a reasonable direct picture of the steepness of the crystallization rate versus temperature (the abscissa and the ordinate, respectively, in Fig. 2b) curve of this material, below its melting point. However, experimental inaccuracies (as illustrated for −16 °C/min) did affect the results, and may, thus, require more detailed analysis of the behavior and of the possible conclusions. Not surprisingly, as expected for any pair of good heating temperature standards, the calibration on heating yields exactly the thermodynamic melting point of the material, for all scanning rate values (cf. upmost part of Fig. 2b).

A liquid crystalline transition of the liquid crystal HP-53, at 93.736 °C, was used to check the calibration on cooling and evaluate its accuracy. The onsets and peak values of the above transition, on heating and cooling, were measured for scans performed over the same sample, at several scanning rates. The peak temperature values of those transitions (normally adopted to characterize them), together with the corresponding error bars, are shown in Fig. 3a. The symmetry (between heating and cooling experiments) of the scanning rate thermal lag is evident. The analysis of this figure may also lead to the very common (but, in our opinion, possible) erroneous conclusion that the supercooling of this liquid crystalline transition is zero.

The results obtained after calibration on heating and cooling, the latter one with Eq. (1), using the melting onsets of indium and lead, are shown in Fig. 3b, together with the standard deviation between the mean and the values obtained in three scans with the same sample. The figure also shows the temperature corrections on heating and cooling when different pairs of standard metals are used, from the set (indium, lead and tin). In Fig. 3b, the open symbols stand for the onset values of the liquid crystalline transition, while the full symbols stand for peak values. A small supercooling, of 0.159 °C, may indeed be identified, even for the lowest scanning rate used, putting into question common assumptions. As a matter of fact, only if no interfaces of any sort and definition are formed in a

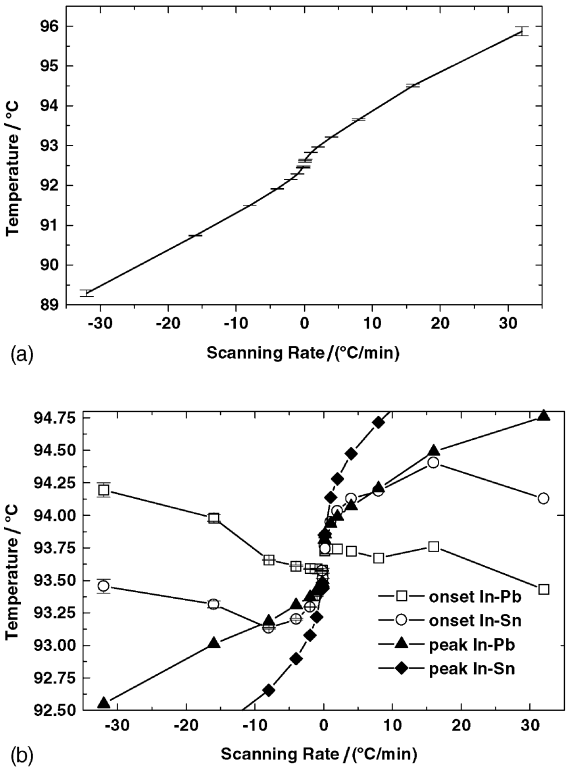

Fig. 3. (a) The peak temperature of the liquid crystalline transition of HP53 on heating and cooling at several scanning rates, before calibration. The error bars are the deviations from the average value for three experiments at each scanning rate. (b) The full symbols are the corrections of the average values shown in Fig. 3a for the peak temperature, after the calibration on heating and cooling, the latter according to Eq. (1). The open symbols would be the results of similar corrections performed over the onset temperature.

phase transition, may one expect zero supercoolings, but (even then) only at strictly zero scanning rate. Also, for the melting and crystallization temperatures of pure metals, one may suspect (and, in our opinion, really expect) that the supercooling can (and will) approach zero only at zero scanning rate, which is entirely consistent with the nucleation theories. With due regard for opposing views, we do not support the assumption that supercooling should be zero for liquid crystals or for any other type of system, with the purpose of directly calibrating dynamic temperature readings in any type of instrument. The issue, however, still requires much closer experimental and theoretical analysis. In the meantime, it clearly appears (and we propose as) wise to avoid the above

Table 1
Temperature shifts when the calibration on cooling is performed, having as reference (for the liquid crystalline transition of HP-53) the extrapolated transition temperature at zero heating rate (93.736 °C)[a]

dT/dt (°C/min)	Onset In–Pb (°C)	Onset In–Sn (°C)	Peak In–Pb (°C)	Peak In–Sn (°C)
−0.1	−0.182	−0.219	−0.260	−0.298
−0.2	−0.158	−0.162	−0.250	−0.254
−1	−0.148	−0.354	−0.312	−0.518
−2	−0.147	−0.439	−0.364	−0.659
−4	−0.125	−0.535	−0.427	−0.839
−8	−0.078	−0.603	−0.553	−1.081
−16	−0.245	−0.421	−0.725	−1.401
−32	−0.459	−0.281	−1.186	−1.944

[a] The values indicated were obtained by subtraction of 93.736 °C from the extrapolated onset (or peak) value at the specified cooling rates.

assumption when devising reliable temperature calibration methods.

The errors with which the calibration on cooling would be performed, at the indicated cooling rates, assuming that the material would always behave as having strictly zero supercooling (which we do not endorse), may be quantified by assuming that the true transition temperature is the one obtained by extrapolation of the heating scans to zero scanning rate, which yields the value of 93.736 °C. Assuming again an efficient heat transfer and a negligible thermal resistance for the liquid crystal, the corrected temperature values of Fig. 3b (note the widely expanded ordinate scale) may give us, either a measure of (let us assume) the genuine errors associated with calibrations performed with such liquid crystal, or the material's genuine supercoolings or superheatings, in cooling or heating scans, respectively. Table 1 shows (only for the cooling scans) the differences between the measured and corrected values and 93.736 °C. They are small, but follow clear, physically interpretable trends with varying scanning rate (particularly those referring to the peak values), which deserve closer analysis and rational interpretation. We therefore suggest that a better measure of the errors incurred in the calibrations may be obtained from the differences (in Table 1) between corresponding In–Pb and In–Sn column values.

The calibration on cooling is particularly important in non-isothermal crystallization experiments, such as those shown in Fig. 4, for the crystallization of polypropylene at scanning rates of −4 and −32 °C/min. The open symbols are the result of integration of the exothermal crystallization peaks obtained with the default DSC calibration (i.e. no calibration). The dashed lines are the shift of the experimental data as a result of the calibration on cooling according to Eq. (1). The full line shows the additional correction, due to the sample's thermal resistance and release of the heat of crystallization. The values used to perform those corrections were $R_s = 40$ K/W, $m = 8$ mg, $\bar{c}_p = 2.09$ J/kg and $|\Delta h_c| = 89$ and 83 J/g for the scans at −4 and −32 °C/min, respectively.

From the above curves, and others at intermediate cooling rates, a temperature, $T_{50\%}$, corresponding to half of the phase change, may be defined. The relationship between this temperature and the kinetic constant of the Nakamura/Avrami equation, usually used in the description on non-isothermal crystallization, is similar

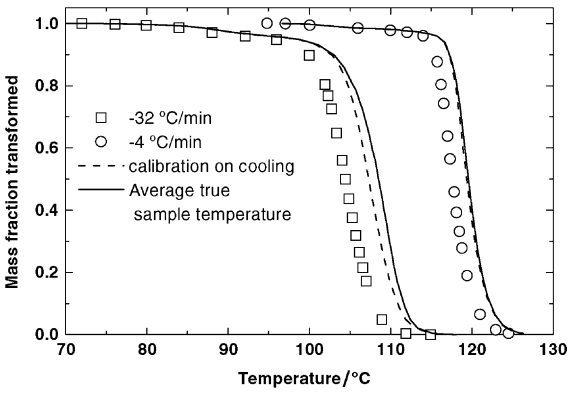

Fig. 4. Non-isothermal crystallization of polypropylene at scanning rates (○) −4 °C/min, and (□) −36 °C/min. Dashed lines are the corrections for the calibration on cooling at the rates indicated. Full lines are the corrections for the sample's thermal resistance and release of the heat of crystallization.

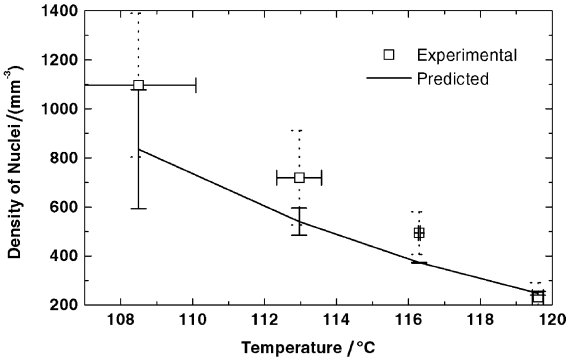

Fig. 5. Experimental values of the density of nuclei plotted against the crystallization temperature and prediction of $\bar{N}_t$ for $T_{50\%}$ (as measured from the curves of Fig. 4 after temperature corrections). The errors with which the calibration on cooling was performed are shown by the horizontal error bars over the symbols and its effect on the evaluation of the average density of nuclei are the dotted vertical error bars over the line. The dotted error bar is the error in the counting of the number of nuclei.

to the one existing between $t_{50\%}$ and k (Eq. (3)):

$$\frac{T_{50\%} - T_m^0}{\dot{T}} = \frac{(\ln 2)^{1/3}}{Z(T_{50\%})} \equiv \left(\frac{\ln 2}{k}\right)^{1/3} = t_{50\%}, \qquad (6)$$

although, in isothermal scans, the time is usually set to zero at the start of the isothermal, and not at the time at which the material crosses its thermodynamic melting temperature.

After the evaluation of $T_{50\%}$ for each one of the scanning rates, Eq. (5) may be used to predict the average density of nuclei for each temperature. The results of the prediction are shown in Fig. 5, where the experimental values, evaluated by optical microscopy, from sections cut from DSC samples crystallized at different cooling rates, are also represented (open symbols). The horizontal error bars over the open symbols are errors in the definition of $T_{50\%}$ resulting from the calibration on cooling. The same error is also reflected in the prediction of the average density of nuclei according to Eq. (5), and is illustrated by the vertical error bars over the full line. An possible source of experimental error is the evaluation of the average density of nuclei from a surface density, according to $\bar{N}_t = (\sigma/1.458)^{3/2}$, where σ is the number of nuclei per unit area, evaluated by directly counting the spherulites in microtomed sample sections [4,12]. Vertical dotted error bars over the open symbols show this particular experimental error, which was evaluated by repeated counting of the number of spherulites in the field of view, at different points of the same section and at different sections of the microtomed sample.

4. Final discussion

The prediction of the average density of nuclei of Fig. 5 deviates from the experimental observations by approximately 20%. Moreover, the error bars between the predicted and experimental values are mostly superimposed. As referred to previously, the vertical error bars in the predicted values are the result of the errors with which the calibration on cooling was performed on the evaluation of the average density of nuclei. An additional error source is certainly the assumption, made in the method for the evaluation of the average density of nuclei, that all the spherulites in the crystallized polymer have an exact spherical shape. Since this last assumption is difficult, if not impossible to circumvent, the first one will be examined in detail, together with other possible error sources always present, and most often neglected, in DSC scans.

The exact magnitude of the errors of the calibration on cooling is difficult to be quantified, due to their dependence on the purity of the liquid crystal and on its thermal resistance and, as argued in the previous section, may be physically interpreted and attributed to the sample's (supercooling) behavior, rather than to errors. The temperature differences shown in Table 1 are only the result of the application of the method used for the calibration on cooling with the melting onsets of pure melting standards. Its applicability is independent of the combination of standard metals used in the calibration. Only pairs of standard metals were used to test the method proposed, mainly because the temperature calibration routine in the Perkin-Elmer DSC-7 allows the use of only two standards. The results of Fig. 3b clearly show that the pairs indium–lead and indium–tin may be used for this purpose.

The effect of the thermal resistance of the liquid crystal, which was not quantified, was not included in the evaluation of the errors. This effect may, however, be important at high cooling rates, where the deviation

between the expected values for different combinations of standards also increases.

The polymer samples' thermal resistances were, however, evaluated, as well as the effect of the heat of crystallization released during the solidification. The result of this correction, shown in Fig. 4, yields a higher value for the temperature $T_{50\%}$ than the one obtained with the calibration on cooling (or with the default DSC calibration). An accurate evaluation of the average true sample temperature, however, requires the knowledge of the temperature profile in the sample, including the sample's bottom and top surface temperatures, their dependence on the sample's thickness and on the scanning rate. In particular, it is important to accurately evaluate the effect that the temperature profile in the sample may have on its crystallization kinetics, in the case of polymers.

For this purpose, a set of experiments and simulations were also carried out in order to evaluate and predict this temperature profile. The experiments were performed in samples with controlled thickness and area, measured before and after a set of experiments with those samples. Since these experiments could not be performed with polypropylene samples, due to the superposition of the melting temperatures of this material and indium, samples of polyethylene (PE), with thickness ranging from 0.25 to 0.64 mm, were used instead (the results being shown in Fig. 6). All samples were round disks with a diameter of 6.3 mm and all of them were encapsulated in 30 μl aluminum pans. The thermal lag between the bottom and top surfaces was measured, as indicated, by measuring the difference between the melting onsets of indium and of indium over the polymer sample. Thin samples with a similar mass of indium were used. The melting onset of indium was measured by performing a calibration check using a sample in a similar aluminum pan as the one used for the polymer sample.

A surprising behavior is observed for the sample with the highest thickness (0.64 mm), for which the resulting thermal lag is smaller. At the temperature where the thermal lag was measured, the sample's dimensions were certainly larger than those measured in the solid state, at room temperature, the expected change being around 15%. This decreasing in the thermal lag on thicker samples was also observed for samples of other polymers. But, contrary to what was assumed previously [14], these experiments

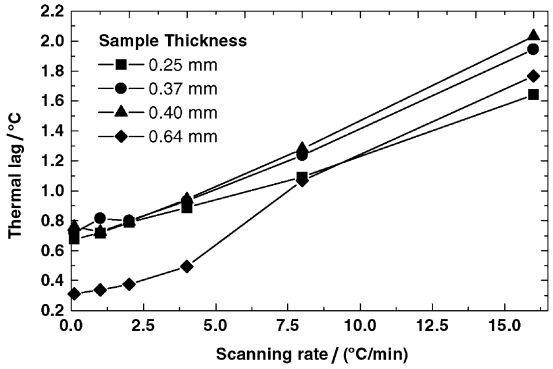

Fig. 6. Measured thermal lag for PE samples with varying thickness at several scanning rates. Aluminum pans of 30 μl were used in all experiments. The thickness values were measured after the experiments.

clearly show that, in heating scans, the top temperature is lower than the bottom temperature.

However, since some doubts could be raised concerning the soundness of the method used to perform these measurements, a computer simulation of the temperature profile in the DSC sample was also performed. It was assumed that the top and bottom of the aluminum pan follow the program temperature and that, inside the pan, the sample is in perfect thermal contact with the pan's material, having at its top a pocket of gas (assumed to be nitrogen), whose thickness changes with the sample in use. The top of the aluminum pan looses heat, by convection, to a cold source, which is assumed to be at 5 °C, i.e. at the cooling block temperature. One-dimensional transient heat transfer conduction through the entire domain was assumed. Because the air gap is of very small size, natural convection will not occur and the region may be assumed as a purely conductive domain.

The heat conduction equation was discretized using a cell-centered finite volume technique and implicit discretization was used in the time derivatives. In this way, all values refer to the center of the cells and the boundary values are related to those in the vicinity by an appropriate interpolation scheme. The polymer and gas thermal properties are assumed temperature independent. Additional details concerning the methodology used and experimental results will be given elsewhere [15].

The results of the simulations are shown in Fig. 7. The parameters used were, for PE, $\rho = 750$ kg/m^3, $c_p = 2800$ J/K kg and $k = 0.3$ W/m K and, for nitrogen,

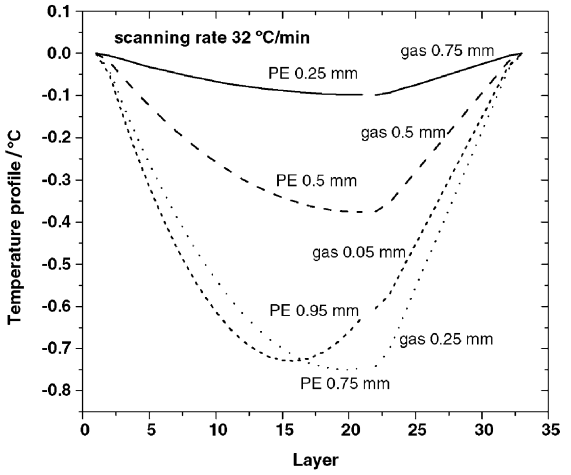

Fig. 7. Simulation of the temperature profile in PE samples with varying thickness.

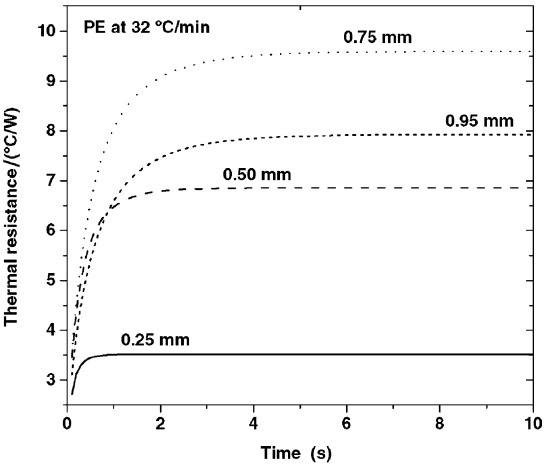

Fig. 8. Calculated PE thermal resistance values for the samples of Fig. 7, at a scanning rate of 32 °C/min.

$\rho = 0.854$ kg/m^3, $c_p = 1042$ J/K kg and $k = 0.0259$ W/m K. Both the experimental and the simulated results show the importance that the sample's thickness may have on the establishment of the temperature profile across the sample and the role played by the gas pocket trapped inside the aluminum pan.

The predicted values for the thermal lag are lower than those of Fig. 6. One reason for this deviation is that the experimental values of Fig. 6 still need to be corrected, since the thermal event used to measure the thermal lag is the supply of the heat of fusion to melt the indium at the top of the polymer sample. This thermal event must be detected by the sensors located at the bottom of the platinum oven, and the pathway will mostly be that of the lowest thermal resistance. For thin samples, most of the heat flux will cross the polymer sample in the bottom–top direction, while for thickest samples, where the thermal resistance of the gas gap is lower than that of the polymer sample, the heat flux may easily be transmitted to the sensors through the aluminum pan.

An idea of the time needed for this detection may be inferred from the results of Fig. 8, where the sample calculated thermal resistance is plotted as a function of time for samples with different thickness. This time is given by the intersection point of two tangent lines drawn at the transient part of the thermal response and at the plateau line, yielding for the 0.50 mm thick sample 0.37 s, which multiplied by the scanning rate (32 °C/min), gives 0.37 °C as the correction needed for the experimental thermal lag at this scanning rate, in accordance with the results of Fig. 7.

The results of Fig. 6 should then also be corrected, for each scanning rate, for the thermal lag caused by the delay in the detection of the thermal event. Work is in progress in order improve the accuracy of the prediction of the temperature profile within the polymer samples and to analyze its effect on the overall crystallization kinetics, and on the assignment of the temperature corresponding to half of the phase change. Nevertheless, the approach used in this work seems to be a good starting point for the above purpose.

5. Conclusions

(1) In addition to proper and specific temperature calibrations on heating and on cooling, sound DSC data treatment and interpretation require accounting for additional sample thermal effects, namely its thermal resistance, phase change heat released/absorbed, and of the resulting sample temperature profiles.
(2) Accurate temperature calibration on cooling is the most difficult to carry out and interpret. The coupling with supercooling effects must be taken into account and carefully quantified. Experimental and theoretical work is still required on this topic, preferably to simple application of common, poorly justified, concepts and procedures.

(3) The present exercise in thermal (DSC) data collection and treatment, with due account for the above specific effects, enabled a physically sound and detailed interpretation of important aspects of polymer crystallization, namely those related with its overall kinetics and density of nucleation.

Acknowledgements

The authors wish to acknowledge Dr. Clara Cramez for having performed the non-isothermal DSC experiments on PE samples, and for the evaluation of the number of nuclei in the DSC sample sections. The acknowledgments are also extended to Dr. Stefan Sarge for supplying small amounts of liquid crystals that were first used in these experiments and Dr. Steffen Neuenfeld, from Merck, for the kind supply of the liquid crystals that were used later on.

References

[1] M.J. Richardson, in: G. Allen, A. Bevington (Eds.), Comprehensive Polymer Science, Vol. 1, Pergamon Press, Oxford, 1989, p. 867.
[2] M.J. Richardson, Thermochim. Acta 300 (1997) 15.
[3] G.W.H. Höhne, W. Hemminger, H.-J. Flammersheim, Differential Scanning Calorimetry: An Introduction for Practitioners, Springer, Berlin, Heidelberg, 1996.
[4] J.A. Martins, M.C. Cramez, M.J. Oliveira, R.J. Crawford, Prediction of the spherulite size in rotationally moulded polypropylene, J. Macromol. Sci. Phys., submitted for publication.
[5] J.A. Martins, J.J.C. Cruz Pinto, Thermochim. Acta 332 (1999) 179.
[6] J.D. Menczel, T.M. Leslie, J. Thermal Anal. 40 (1993) 957.
[7] J.J.C. Cruz Pinto, Notes on the calibration on heating and cooling of differential scanning calorimeters, Report, 1997, Universidade de Aveiro, Aveiro, Portugal.
[8] J.A. Martins, N.M. Alves, J.F. Mano, J.J.C. Cruz Pinto, Thermochim. Acta 369 (2001) 175.
[9] J.A. Martins, J.J.C. Cruz Pinto, Polymer 41 (2000) 6875.
[10] M.C. Cramez, A study on the microstructure and properties of rotationally moulded plastics, Ph.D. Thesis, Universidade do Minho, 2000.
[11] J.D. Hoffman, G.T. Davis, J.I. Lauritzen Jr., in: N.B. Hannay (Ed.), Treatise on Solid State Chemistry, Vol. 3, Plenum Press, New York, 1976, p. 497.
[12] J.A. Martins, J.J.C. Cruz Pinto, Evaluation of the instantaneous nucleation density in the isothermal crystallization of polymers, Polymer (2002), in press.
[13] S.M. Sarge, G.W.H. Höhne, H.K. Cammenga, W. Eysel, E. Gmelin, Thermochim. Acta 361 (2000) 1.
[14] S.L. Simon, Macromolecules 30 (1997) 4056.
[15] J.A. Martins, M.J.A. Malheiro, J.C. Teixeira, J.J.C. Cruz Pinto, in preparation.